Soft Matter

Accepted Manuscript

This article can be cited before page numbers have been issued, to do this please use: M. Ahmadi, S. Pioge, C. Fustin, J. Gohy and E. van Ruymbeke, *Soft Matter*, 2016, DOI: 10.1039/C6SM02576E.

ROYAL SOCIETY OF CHEMISTRY

rsc.li/soft-matter-journal

View Article Online
DOI: 10.1039/C6SM02576E

Journal Name

ARTICLE

Closer insight in the structure of moderate to densely branched comb polymers by combining modelling and linear rheological measurements

Received 00th January 20xx,
Accepted 00th January 20xx

DOI: 10.1039/x0xx00000x
www.rsc.org/

Mostafa Ahmadi[a*], Sandie Pioge[b], Charles-Andre Fustin[c], Jean-Francois Gohy[c], Evelyne van Ruymbeke[c]

Synthesis of combs with well-entangled backbones and high densities of long branches has always been a challenge. Steric hindrance frequently leads to coupling of chains and structural imperfections that cannot be easily distinguished by traditional characterization methods. Researches have therefore tried to use combination of different methods to have more information on the actual microstructures. In this work, a grafting-from approach is used to synthesize poly(n-butyl acrylate) combs using Atom Transfer Radical Polymerization (ATRP) in three steps including synthesis of backbone, cleavage of protecting groups and growth of side branches. We have compared the theoretical prediction of linear viscoelastic properties made by time marching algorithm (TMA) tube based model with measured rheological behaviour to provide a better insight on the actual microstructure formed during synthesis. For combs with branches smaller than an entanglement, no discernible hierarchical relaxation can be distinguished, while with longer branches, a high frequency plateau made by entangled branches can be separated from backbone's relaxation. Dilution of backbone, after relaxation of side branches, may accelerate final relaxation, while extra friction can delay it especially for longer branches. Such a comparison provides a better assessment of the microstructure formed in combs.

I. Introduction

Comb architecture is one of the important chain microstructures that is frequently encountered in different polymerization systems. Metallocene catalysts are capable of incorporating in-situ formed macromonomers into the growing chains, leading to formation of sparsely branched combs.[1] Post-modification of polyethylene using peroxides during process, as well as irradiation using high energy beams, can lead to formation of moderate to highly branched comb-like structures.[2] However, these examples provide low degree of control on the formed branching structure and may lead to polydisperse polymers. Particular synthesis approaches have therefore been developed for the controlled synthesis of well-defined comb-like structures due to their specific applications.[3] The classical approach for the synthesis of controlled complex molecular structures is the well-known anionic polymerization which is limited to specific monomers and involves stringent polymerization conditions such as high purity of reaction components and very low concentration of contaminants. Developments in controlled radical polymerization (CRP) have opened new opportunities for the synthesis of complex architectures from a broader range of monomers and under milder reaction conditions.[4] Atom transfer radical polymerization (ATRP), reversible addition-fragmentation chain transfer (RAFT) and nitroxide mediated polymerization (NMP) are among the most widely used CRP methods for synthesis of well-defined structures. Step-wise approaches using one type of the mentioned methods or combination of different CRP methods have been successfully applied to synthesis of complex structures such as combs and brushes.[5-8] Application of different chemistries for different parts of comb and brush architectures has led to different graft polymers with specific morphologies and stimuli responsiveness.[5, 6, 8]

Three approaches have been widely used for synthesis of comb and brush structures: "grafting-onto", i.e. attachment of side branches to the backbone using complementary functional groups, "grafting-through", i.e. (co)polymerization of macromonomers, and "grafting-from", i.e. growth of side branches from a macro-initiator backbone.[9] Each of these methods has its own pros and cons. Grafting-through affords predetermined branch length and density, but there are limitations on the backbone length especially when high branching density is desired.[10-13] Grafting-from approach has disadvantage of lower control on the length of side branches but gradual growth of branches removes the steric hindrance issues and gives a better control on branching density.[5-7] This method also suffers from intermolecular side reactions that may lead to coupling of combs specially at high branching length and densities.[7] Grafting-onto allows the control on the number and length of side branches, while suffers from limited branching density due to steric hindrance.[14, 15] Since the microstructure of the synthesized combs has a significant effect on their properties and applications, each of the mentioned approaches might be useful in their places. Depending on the length of the backbone and side branches,

[a] *Department of Polymer Engineering and Color Technology, Amirkabir University of Technology, Tehran, Iran.*
[b] *Institute des Molécules et des Matériaux du Mans, Université du Maine, Le Mans, FRANCE.*
[c] *Bio and Soft Mater Division (BSMA), Institute of Condensed Matter and Nanosciences (IMCN), Université catholique de Louvain, Louvain-la-Neuve, Belgium.*

† Footnotes relating to the title and/or authors should appear here.
Electronic Supplementary Information (ESI) available: [details of any supplementary information]. See DOI: 10.1039/x0xx00000x

View Article Online
DOI: 10.1039/C6SM02576E

they can exhibit unique macroscopic topologies and transform from star- to brush-like polymers.[10, 12] Most of the reported synthesized combs had short backbones especially when high branching length and densities were desired, and longer backbones have been associated with shorter branches or lower branching densities.[12, 16] In fact, synthesis of combs with long and well-entangled backbones, i.e. at least with ten entanglement length, and high densities of long branches, i.e. branches with more than an entanglement length and less than an entanglement distance, has always been a challenge.

Although the most accurate synthetic approaches have been used for synthesis of comb and brush architectures, coupling of chains and structural imperfections cannot be easily distinguished by regular characterization methods like size exclusion chromatography (SEC). Combs with different number and length of branches can have similar hydrodynamic volume and hence cannot be separated using traditional fractionation techniques. Moreover, densely branched combs and brushes with extremely high molar masses show anomalous elution behaviour and elute on larger elution volumes in SEC.[17] Therefore many researches have tried to combine different methods to have more information on the actual microstructures. In particular, new separation techniques like Temperature Gradient Interaction Chromatography (TGIC) are coupled with modelling and rheology as complementary tools in characterizing a complex polymer.[14, 18, 19]

Architectural characteristics of complex structures have long been known to display a clear signature on the rheological properties. As complex architectures relax hierarchically, sequential relaxation steps have separate signatures in the relaxation spectrum.[14, 20-23] On the other hand, there has been a remarkable progress in theoretical description of the rheology of complex polymers.[24-27] Tube-based models have proved to be sufficiently accurate in order to be used as complementary tool for the inverse problem of characterizing a complex polymer structure according to their rheological behaviour.[14, 18, 19]

This work is focused on the rheological properties of moderate (with one entanglement distance between branches) to densely branched combs having well-entangled backbone (with ten entanglement length). Grafting-from approach is used to synthesize poly(n-butyl acrylate) (PnBA) combs using ATRP in three steps including (a) synthesis of backbone copolymer (b) cleavage of the protecting groups to provide multi-functional macro-initiator and (c) growth of side branches. Theoretical prediction of linear viscoelastic properties are made by time marching algorithm (TMA) tube based model developed previously,[24] and the results are compared with measured rheological behaviour to provide a better insight into the actual microstructure formed during synthesis.

II. Experimental

II.1 Materials

n-butyl acrylate (nBA, 99 %) was purchased from Aldrich and purified by passing through a column of basic alumina. Unstabilized trimethylsiloxy protected ethyl acrylate (HEA-TMS, 97%) was purchased from abcr and was used without any purification. Ethyl 2-bromopropionate (EBP, 98%), *N,N,N′,N″,N″*-pentamethyldiethylenetriamine (PMDETA, 99 %) and copper (I) bromide (CuBr, 99,999%) were purchased from Aldrich and used without extra purification. The rest of used materials were commercially available, synthesis grade and were used without further purification.

II.2 Characterization

Monomer conversions and copolymer compositions were determined by proton nuclear magnetic resonance (^{1}H NMR) spectroscopy. ^{1}H NMR spectra were recorded on a Bruker Avance 2 spectrometer operating at 300 MHz. Chemical shifts were reported downfield from tetramethylsilane in $CDCl_3$ as the internal standard at room temperature.

The average molar masses (number-average molar mass $\overline{M_n}$, weight-average molar mass $\overline{M_w}$) and dispersity ($Đ = \overline{M_w}/\overline{M_n}$) were determined using a Waters gel permeation chromatography (GPC), Waters 410 refractometer as the detector and Waters WISP 712 autoinjector with injection volume of 150 µL using three PLgel 5µ columns: 10^2 Å, 10^3 Å and 10^4 Å. Tetrahydrofuran (THF) stabilized by BHT, with flow rate of 0.8 mL/min at 30 ˚C was used as the eluent. Relative molar masses were determined using a calibration curve based on polystyrene standards.

Linear viscoelastic (LVE) properties of the samples were measured using an ARES rheometer from TA instrument with 8 mm diameter parallel plate geometry and 0.5 to 1 mm gap, under strain controlled mode. The tests were carried out at temperatures between -20 and 80 ˚C under nitrogen atmosphere to reduce the risk of degradation. The original gap was adjusted at each temperature for density changes in sample and instrument. Strain sweeps were carried out for each sample at constant frequency of 1 rad/s in order to determine the linear viscoelastic region for frequency sweep measurements. Master curves were obtained at reference temperature of 25 ˚C based on time-temperature superposition principle and the shift factors were determined using William-Landel-Ferry (WLF) equation.

II.3 Synthesis

Linear PnBA homopolymers. In a 25 mL schlenk flask, anisole (4.12 mL, 25% v/v, for the case of L145) as the solvent and the internal standard of ^{1}H NMR measurements, EBP (7.2 µL, 55.2 µmol) as the initiator, nBA as the monomer (12.35 mL, 86.2 mmol) and PMDETA (11.5 µL, 55.2 µmol) as the ligand were added and the resulting solution was bubbled with argon (Ar) for 30 minutes. CuBr (7.9 mg, 55.2 µmol), as the catalyst, was added to a 25 mL round-bottom flask, the flask was degassed by vacuum and the internal atmosphere was replaced by Ar. The solution was transferred to the catalyst containing vessel and was placed in an oil bath at 80 °C. During polymerization, sampling was performed with a degassed syringe in order to determine the conversion using ^{1}H NMR. After reaching the desired conversion, the reaction was stopped by cooling and opening the flask to air, and mixture was dissolved in CH_2Cl_2 and passed through a column of natural alumina in order to remove the copper complex. The solution was precipitated in an excess amount of methanol and the precipitate was dried under vacuum.

Linear P(nBA-*co*-HEA) copolymers. The overall procedure was the same as the homopolymerization of nBA described before except that 10% v/v of anisole was used as solvent and different molar ratios of BA and HEA-TMS were used in order to prepare copolymers with different comonomer compositions. For the case of BB4, SEC : Mn = 143 kg/mol, Đ=1.19; ^{1}H NMR ($CDCl_3$, δ in ppm): HEA-TMS peaks (ppm): 0.13 (s, Si(**CH_3**)$_3$), 1.7 and 1.9 (m, **CH_2** in polymer main chain), 2.34 (m, **CH** in polymer main chain), 3.75 (m, **CH_2**-OSi), 4.10 (m,

View Article Online
DOI: 10.1039/C6SM02576E

C(O)O-**CH_2**); BA peaks : 0.95 (t, **CH_3**), 1.36 and 1.6 (m, 2**CH_2**), 1.7, 1.9 and 2.3 (m, **CH_2** and **CH** in polymer main chain), 4.0-4.1 (m, C(O)O-**CH_2**). Composition (^{1}H NMR): BA/HEA-TMS = 96/4.

Multi-functional P(nBA-*co*-BPE) macroinitiators. The random copolymer of P(nBA-*co*-HEA) (4.37 g, 1.2 mmol, for the case of BB4) produced in the previous step was placed in a 25 mL round-bottom flask and dissolved in THF. The solution was bubbled with Ar for 30 minutes. Potassium fluoride (KF, 69.6 mg, 1.2 mmol) was added followed by dropwise addition of tetrabutylammonium fluoride (TBAF, 3.5 µL, 12 µmol) and subsequent slow addition of 2-bromopropionate bromide (BPB, 0.19 mL, 1.8 mmol). The reaction mixture was stirred at room temperature for 24 hours. The product was then dissolved in THF, passed through a column of basic alumina and the solvent was removed by rotary evaporator. A concentrated solution of the macro-initiator in THF was precipitated in methanol. ^{1}H NMR ($CDCl_3$, δ in ppm): in addition to BA peaks: 1.7 and 1.9 (m, **CH_2** in polymer main chain), 1.82 (d, Br-CH-**CH_3**), 2.34 (m, **CH** in polymer main chain), 4.15 (m, O-**CH_2**-CH_2-OCO-CH-Br), 4.36 (m, O-CH_2-**CH_2**-OCO-CH-Br), 4.52 (m, Br-**CH**-CH_3).

Comb PnBA-*g*-PnBA homopolymers. Desired amount of P(nBA-*co*-BPE) macro-initiator (0.4 g, 0.12 mmol, for the case of C4 series) was placed in a 25 mL round-bottom flask and dissolved in anisole (1 mL, 10% v/v). PMDETA (25.6 µL, 0.12 mmol) and nBA (8.8 mL, 61.4 mmol) were added and the solution was bubbled with Ar for 30 minutes. CuBr (17.6 mg, 0.12 mmol) was added to another 25 mL round-bottom flask and degassed with Ar. The solution was transferred to the catalyst vessel and the flask was placed in an oil bath at 70˚C. A sample was removed in order to be used as the reference for later calculation of conversions during polymerization using ^{1}H NMR. After desired conversion, the reaction was opened to air, the product was dissolved in CH_2Cl_2 and passed through a column of natural alumina. The solvent was removed by rotary evaporator, the polymer was precipitated in methanol and dried under vacuum. ^{1}H NMR ($CDCl_3$, δ in ppm): 0.95 (t, **CH_3**), 1.36 and 1.6 (m, 2**CH_2** in BA units), 1.7 and 1.9 (m, **CH_2** in polymer main chain and side branches), 2.34 (m, **CH** in polymer main chain and side branches), 4.0-4.10 (m, C(O)O-**CH_2** in BA units), 4.10 (m, C(O)O-**CH_2**-**CH_2** in side branches).

III. Results and Discussion

III.1 Synthesis and Characterization

Conventional free radical polymerization of acrylate monomers leads to undefined branched structures.[28] Depending on concentration of the growing radicals in the reaction media, inter- and intra-molecular chain transfers may lead to long and short branches, respectively. In most of the cases the simultaneous variations in molar mass, dispersity and structure of branches lead to complex rheological behaviours.[29] This might be the reason why rheological studies on acrylates are so rare. In this contribution, we use a grafting-from approach based on an ATRP mechanism to synthesize well-defined PnBA combs in which the length of the PnBA backbone, the number of grafted PnBA chains and the length of the PnBA grafts can be controlled by tuning the experimental conditions. The three steps ATRP approach to synthesis of PnBA combs as explained in the previous section, are illustrated in Scheme 1.

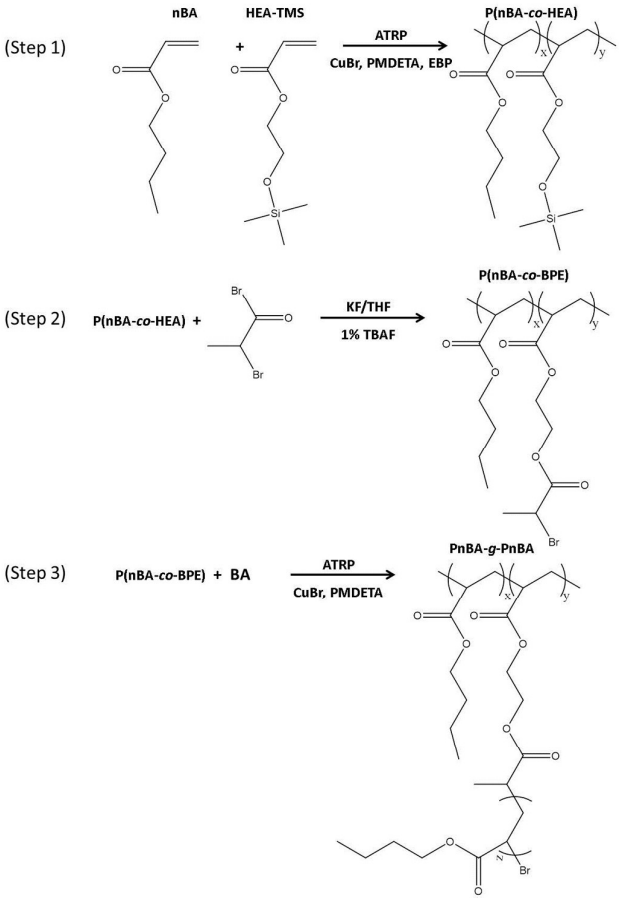

Scheme 1. ATRP approach to synthesis of PnBA combs using a grafting-from method.

First, copolymers with different comonomer fractions were synthesized to be used as the backbones of the combs (BB1, BB4 and BB7). Since both nBA and HEA-TMS belong to the acrylate monomer family, we expect similar reactivities and thus a random distribution of comonomers. Homopolymers (L45 and L145) were synthesized to be used as references for later rheological studies. Details of reaction conditions and the molecular characteristics of the final products are depicted in Table 1.

Table 1. Reaction conditions and characterization results of linear polymers.

Sample	[M]:[EBP]:[Cu]:[PMDETA]	Conversion[a] (%)	HEA[a] (mol%)	Mn_{SEC}[b] kg/mol	Mn_{NMR}[c] kg/mol	Đ[b]
L45	500:1:1:1	57	-	44	37	1.13
L145	1500:1:1:1	73	-	144	140	1.13
BB1	1500:1:1:1	64	1	149	124	1.13
BB4	1500:1:1:1	63	4	143	123	1.19
BB7	1500:1:1:1	65	7	143	129	1.13

View Article Online
DOI: 10.1039/C6SM02576E

[a] determined by ^{1}H NMR spectroscopy. [b] measured by SEC with polystyrene standards. [c] calculated from conversion.

Figure SI2 shows the ^{1}H NMR spectrum of the purified P(nBA-*co*-HEA). The final copolymer compositions were determined by ^{1}H NMR spectroscopy. The integration area of OCH_2 from nBA and HEA-TMS units (labelled a and e) and 9 protons of trimethylsiloxy group around 0.13 ppm (labelled g) from HEA units were compared to get final copolymer composition. Comonomer fractions were 1, 4 and 7, that will deliver moderate to densely branched combs.

Relative molar masses were measured by SEC and results are depicted in Table 1. The measured molar masses are in good agreement with the expectations from reaction's conversion. All of the samples have very low Đ (less than 1.19) and high molar masses (about 150 kg.mol^{-1}) which reveal the efficiency of ATRP to control reaction kinetics and attain high molar mass chains (see Figure SI3 for Molecular Weight Distribution (MWD)). The ^{1}H NMR results of comonomer compositions were used to calculate the average number of branches per backbone (q = DP × HEA%) in each series of combs, which led to 10, 34 and 68 branches in each comb series.

The second step involves the cleavage of protective groups and grafting of initiation sites for ATRP of branches. The multi-functional poly(nBA-*co*-(2-(2-bromopropionyloxy)ethyl acrylate)) (P(nBA-*co*-BPE)) macroinitiators were synthesized by reacting the P(nBA-*co*-HEA) with BPB in the presence of KF and TBAF as the catalytic system in THF at room temperature (Scheme 1) and were characterized by ^{1}H NMR and SEC. Figure 1 compares the ^{1}H NMR spectra before and after esterification. The removal of HEA-TMS characteristic peaks at 0.1 and 3.85 ppm (labelled g and f) and appearance of new peaks from 4.15 to 4.5 ppm confirms the esterification reaction. The integration area of OCH_2 at 4.2 ppm (labelled a and e) from nBA and HEA and the five protons from BPE: Br-CH-CH_3 (labelled l) at 4.52 ppm, O-CH_2-CH_2-OCO-CH-Br (labelled j) at 4.36 ppm and O-CH_2-CH_2-OCO-CH-Br (labelled k) at 4.15 ppm, were compared to calculate the extend of functionalization. The quantitative compensation of the removed HEA-TMS characteristic peaks with the newly appeared ones for all of the samples demonstrates complete esterification of -TMSO groups with BPB. Since the macroinitiators are the backbone of the combs, extensive characterization of MWD and comonomer composition was needed. SEC results confirmed that no degradation happened during esterification.

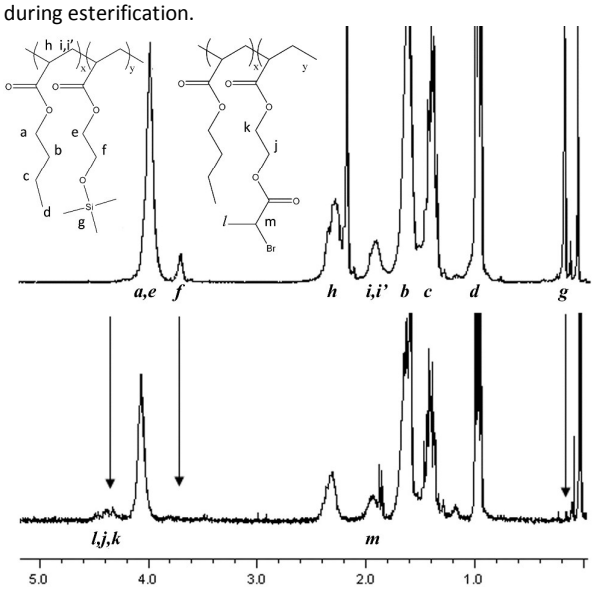

Figure 1. ^{1}H NMR spectra of linear copolymers, before (a) and after (b) functionalization.

Finally the side branches were grown by ATRP of nBA using the multi-functional macro-initiator and CuBr/PMDETA catalytic system at 75 °C (Scheme 1, Figure SI4). Details of polymerization conditions and final characteristics of products are listed in Table 2. Sample codes of Cx-y are used in Table 2, where x refers to the comonomer content of the backbone and y gives the molar mass of the branches in kg/mol. The ratio of monomer to initiator remained constant at 500:1 except for the 1% macro-initiator where the amount of initiation sites was too low and excess monomer had to be used to dissolve the backbone.

Figure 2 shows MWDs of the comb series and the corresponding backbones. The MWD peak broadens and shifts toward higher molar masses as the length of side branches increases. Deconvolution of MWD curves into several log normal distributions can be useful to study the variation of different parts of the peaks as conversion proceeds. Deconvoluted peaks are depicted in Supporting Information Figure SI5 to SI7, and results are summarized in Table SI1. All samples clearly possess a low molar mass shoulder. In addition, some of the samples have coupled combs at higher molar masses.

The low molar mass shoulders in C1-9 and C1-21 samples (Figure SI5) have molar masses of ~50 and ~109 kg/mol, and their corresponding weight fractions are ~4% and ~13%, respectively. The average length of side branches can be calculated based on conversion measurements, assuming that all initiation sites have successfully participated in the second ATRP step, as depicted in Table 2. The initial monomer to initiator molar ratio and the measured conversions yielded lengths of 8.7 and 21.4 kg/mol, for C1-9 and C1-21, respectively.

Several reasons can be postulated as the origin of the low molar mass shoulders. Since the fraction of comonomer is low in this series, the presence of unfunctionalized or dead chains can be one possibility. Another possibility is the hydrolysis of some branches. However, the difference in the molar masses of shoulders and of branches reveals that this statement is wrong, unless not all the initiation sites have found the chance to grow branches. Despite the records in literature on separation of such an impurity by simple solution precipitation procedures,[11] the attempts for removing the low molar mass linear fractions by successive dissolution in solvents and precipitation in non-solvents failed due to closeness of molar masses, which leads to similar thermodynamic driving force for dissolution and precipitation of both parts.

View Article Online
DOI: 10.1039/C6SM02576E

Table 2. Reaction conditions and molecular characteristics of synthesized combs.

Sample	[BA]:[I]:[Cu]:[PMDETA][a]	Conversion (%)	$Mn_{,SEC(comb)}$[b] kg/mol	Đ	$Mn_{,NMR(branch)}$[d] kg/mol	N_{br}[e]	ϕ_{br}[f](vol.%)
C1-9	1000:1:1:1	6.8	191	1.28	8.7	10	36.9
C1-21	1000:1:1:1	16.7	228	1.62	21.4	10	59
C4-4	500:1:1:1	6.9	273	1.34	4.4	34	51.1
C4-7	500:1:1:1	10.5	307	1.46	6.7	34	61.4
C4-13	500:1:1:1	20.5	292	1.78	13.2	34	75.8
C4-19	500:1:1:1	29.7	274	2.55	19	34	81.9
C7-11	500:1:1:1	16.5	396	1.88	10.5	68	83.3
C7-28	500:1:1:1	43	393	2.87	27.5	68	92.9

[a] In 10% v/v of anisole. [b] Determined by SEC, polystyrene standards. [c] Mn of the backbones (from Table 1). [d] Mn of the side branches: calculated based on the initial [BA]/[I] ratio and the corresponding final conversions. [e] Number of side branches: calculated according to composition of the backbones measured by ^{1}H NMR (from Table 1). [f] weight fraction of branches.

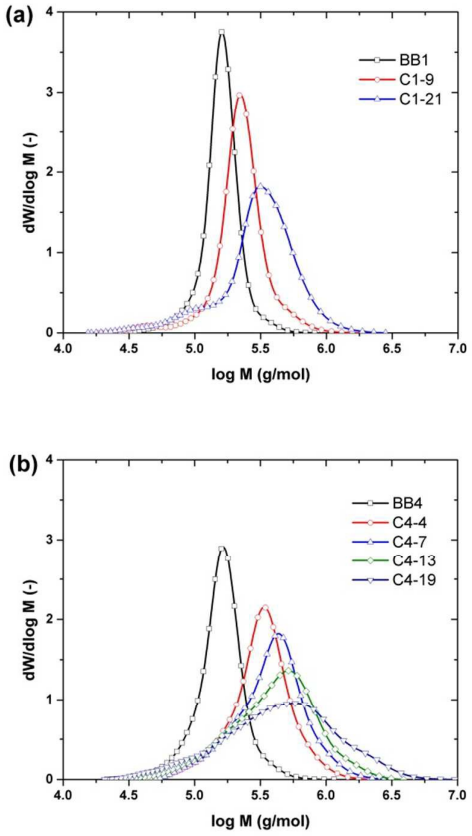

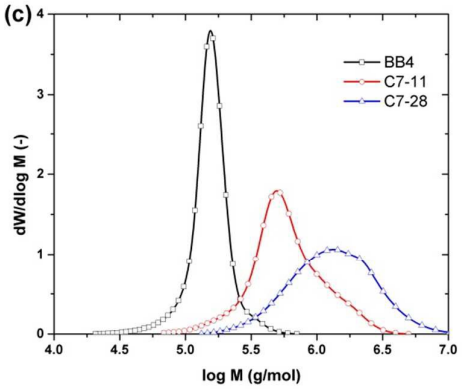

Figure 2. SEC traces of (a) C1, (b) C4 and (c) C7 comb series and corresponding backbones.

MWDs of the C4 series are compared in Figure 2b and SI6. The whole peak shifts toward higher molar masses as the length of side branches increases, but the number average molar masses are almost constant (Table 2) which is due to gradual increase of peak width, especially in the low molar mass region. The presence of high molar mass shoulder is also evident in some samples like C4-13 and C4-19 which can be attributed to intermolecular coupling reaction between growing side branches.[11] The fraction of coupled combs increases from 1% to 2% as the length of side branches increases, and the corresponding average molar masses are ~1800 and 2400 kg/mol that considering the molar mass of the main peak, can be attributed to three coupled combs. Chambon et al. have shown that the presence of about 10% of coupled combs has a minor effect on overall relaxation behaviour of their sparsely branched combs.[14] Excluding the supposed linear fractions and coupled combs, there is a steady increase in the Mn of the main combs in C4 series from 370 to 720 kg/mol (Table SI1). The calculated molar masses exactly match with the summation of molar masses of all branches and backbone. This is not surprising since contraction of polymer coil due to branching relative to the analogue linear chain normally compensates the backbone's stiffening due to special restriction in comb architectures, so that the segment density remains almost the same.[30]

View Article Online
DOI: 10.1039/C6SM02576E

The presence of coupled combs is more evident in C7 series (Figure SI7), and their weight fraction is ~20%. This was anticipated as a higher number of growing branches increases the possibility of intermolecular coupling reaction. Besides, the very long backbone length used in this work, significantly amplifies the branch coupling. Precise observation of SEC data reveals that even at low Đ values, considerable fractions of free linear and coupled combs should be expected, whose fractions increases with increasing branch length. However, we cannot be definite about the number and length of the branches. In the remaining part of this contribution we try to resolve this issue by comparing measurements to the predictions of linear rheological properties.

III.2 Rheological Properties

Rheological properties of acrylate polymers are important characteristics in their special applications such as in paint and adhesive industries. Surprisingly there is not so much rheological data for the case of PnBA. Jullian et al. have recently investigated the rheological properties of linear PnBAs synthesized by ATRP method in order to rectify this gap.[31] They have reported $\boldsymbol{G_N^0}$, of 7.8×10^4 Pa measured at frequency were tanδ shows a local minimum, for the sample with the highest molar mass (4600 kg/mol), and M_e of 26 kg.mol^{-1} according to Graessley's definition.[32] Similar values have been also proposed by Former et al. for the case of branched PnBA.[29] On the other hand Ahmad et al.[33] have reported $\boldsymbol{G_N^0}$ of 1.2×10^5 Pa as the mean value for their branched PnBAs and Pakula et al.[16] have suggested 1.3×10^5 Pa for their comb PnBAs which implies M_e of about 16 kg/mol. This is in agreement with results of Fetters et al.[32] who have reported M_e of 7.7 and 15.2 for poly(ethylacrylate) and poly(octylacrylate) based on persistent length definition, respectively.

Figure 3 shows the master curves of dynamic moduli as a function of frequency at the reference temperature of 25 ˚C for linear homopolymers. There are several methods for extraction of $\boldsymbol{G_N^0}$ from LVE spectra.[34] We used the INT method of Liu et al. which is based on integration of loss modulus in the whole frequency domain:[34]

$$\boldsymbol{G_N^0 = \frac{2}{\pi}\int_{-\infty}^{+\infty} G''(\omega) d ln\omega}$$

Using our high molar mass linear sample and reconsidering Jullian et al.'s 40, 100, and 220 kg/mol samples, we came up with the $\boldsymbol{G_N^0}$ value of ~1.5×10^5 Pa, which corresponds to Me of about 15 kg/mol. Predictions made by tube based models also gave a better fit using combination of these values compared to the previously reported data.

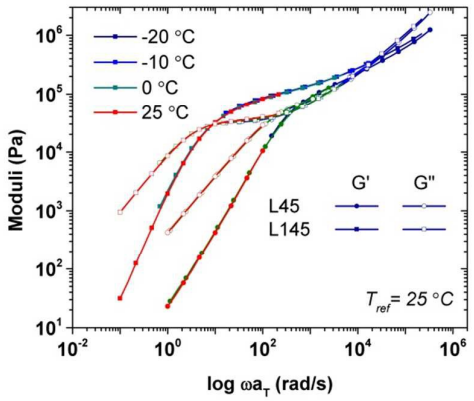

Figure 3. Master-curves of the measured dynamic moduli of linear PnBAs.

Notably, the dynamic moduli of all backbones are nicely superimposable to the moduli of reference linear homopolymer. In other words, the chemical composition did not induce any phase separation or other sources of variation in rheological behaviour. Figure 4 shows the van Gurp-Palmen (vGP) plots of frequency sweep measurements on comb series performed at different temperatures. While the linear chains, as well as branched chains with uniform structures are demonstrated to be thermorheologically simple, combination of linear and different branched structures are reported to show complex behaviour.[35, 36] Our synthesized samples also show progressive failure of time-temperature superposition by increasing the length of side branches, but the overall thermorheological complexity is not significant. Therefore, best fit master curves were built at the reference temperature of 25 ˚C without using any vertical shift and the results are depicted in Figure 5.

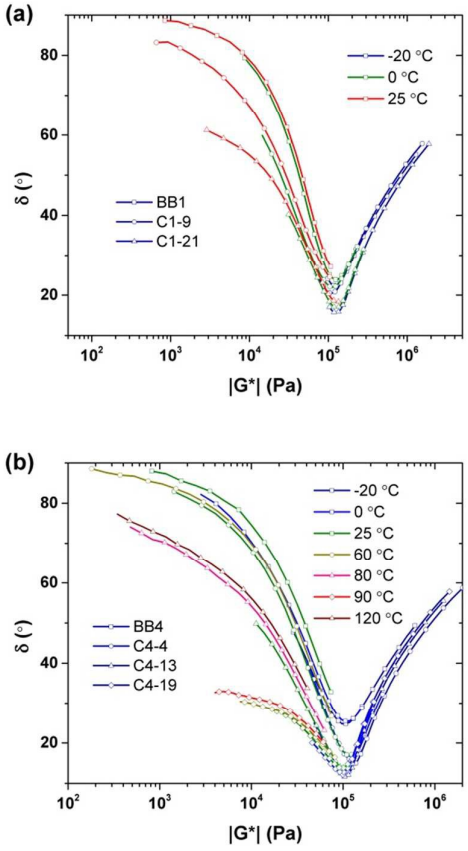

View Article Online
DOI: 10.1039/C6SM02576E

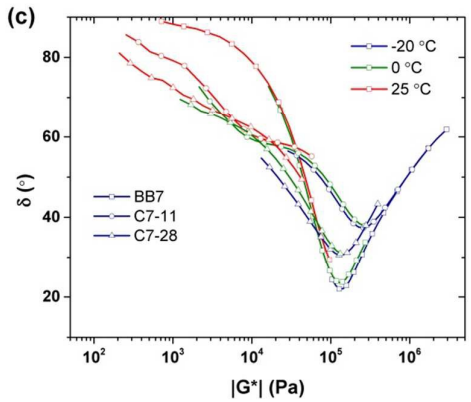

Figure 4. vGP plots of frequency sweep measurements on comb series (a) C1, (b) C4, and (c) C7 at different temperatures as indicated in legends.

Stress relaxation in complex architectures like combs happens hierarchically.[20-24] At early times, stress will be relaxed by unconstraint Rouse motions of the side branch tips and free ends of the backbone. Deeper fluctuations closer to the branching points become exponentially slower as the entropic barrier becomes more than the thermal energy of the system. Branches have two opposite effects on relaxation of the backbone: acceleration due to dilation of the confining tube, and at the same time retardation due to extra friction coming from the disoriented branches.[20, 24] Fluctuations of the backbone segments beyond the first branching point start in parallel with branches, while the inner segments should wait for complete relaxation of all branches. Finally, reptation, delayed by the extra friction from relaxed side branches, may happen in the dilated tube.

Each relaxation step can make its own signature in the relaxation spectrum if their corresponding characteristic times are well separated. Ideally two plateaus should be seen, before and after relaxation of side branches. The second plateau belonging to the still oriented backbone is reduced due to dilution effect as $G^0_{N,2} \propto G^0_{N,1}\varphi^{1+\alpha}$ (1 and 2 indices refer to the first and second plateaus toward lower frequencies) where φ is backbone's volume fraction and α is dilution exponent. Each of these plateaus corresponds to a local minimum in tanδ. However, in reality, depending on the length of the backbone and length and number of side branches, each of these signatures may fade or be overlapped. Combs with short backbones and long side branches resemble star behaviour.[10] In such a case relaxation mechanism does not depend on number of branches. After fluctuation of the branches, the diluted short backbone may relax by simple Rouse mechanism. In such a case only one plateau will be seen due to branch entanglements. Densely branched combs with short branches and long backbones resemble stiff linear chain.[16, 37-39] The plateau modulus will be suppressed and entanglement molar mass will be increased due to large weight fraction of polymer incorporated in side branches. The sole plateau seen in this case originates from entangled backbones.

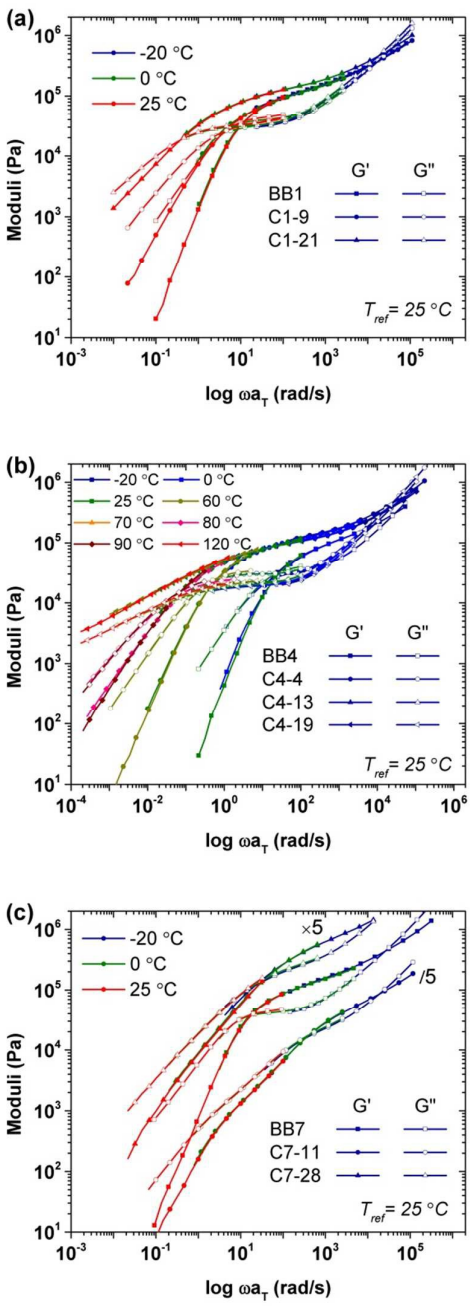

Figure 5. Master-curves of the measured loss and storage moduli of (a) C1 (b) C4 and (c) C7 comb series.

The expected comb-like behaviour, i.e. appearance of two separate plateau moduli corresponding to entangled branches and backbone, cannot be seen in our comb samples. The main reasons are the structural dispersities as described in the previous section and the short length of backbone whose relaxation is not well separated from branches relaxation. Instead, the terminal crossover is postponed to lower frequencies and the terminal slopes of 1 and 2, for respectively loss and storage moduli, are decreased for combs having longer branch. The crossover of C4-19 sample is even shifted to below the accessible frequency window. This behaviour is characteristic of gels and has been previously reported for crosslinked comb networks, as well.[40]

View Article Online
DOI: 10.1039/C6SM02576E

The LVE properties of C7 comb series show the hierarchical relaxation mechanism explained before, as shown in the corresponding moduli and vGP plots. The length of side branches in C7-11 is expected to be less than one entanglement; however a clear separate relaxation of side branches can be distinguished at high frequencies. The linear BB7 backbone with about ten entanglements reptates at least one decade later than complete fluctuations of the side branches in C7-11. After removal of oriented side branches, the backbone is diluted with 0.83 weight fraction of relaxed parts, now acting as solvent. With a six-fold increase of M_e ($\boldsymbol{M_e(t) = M_e(0)\varphi^{\alpha}}$), we can barely see the signature of backbone reptation. Instead, a delayed Rouse-like relaxation can be distinguished. By increasing the length of side branches to almost two entanglements in C7-28, relaxation of branches and the backbone are more separable and the terminal relaxation is postponed to lower frequencies.

The relaxation of free linear chains with at most 18% weight fraction (in C4 series) is hardly recognizable at high frequencies. Their relaxation might be faded by high dispersity in the length of branches that lead to gradual decay instead of a sharp drop at their fluctuations time. The coupled combs at most 20% weight fraction (in C7 series) on the other hand may not be perceptible in the experimentally accessible relaxation frequencies. After relaxation of branches and individual combs, the remaining entangled backbone's of coupled combs form less than 3.2% and even 1.3% weight fraction of oriented chains, for respectively C7-11 and C7-28, that may appear at modulus levels below 150 Pa. Therefore, as described by Chambon et al.[14] such fraction of coupled combs does not have a discernible effect on the relaxation modulus.

The zero-shear rate viscosity of branched polymers dramatically depends on structural parameters of the complex structure. Using tube based models, the backbone length, number and length of branches are quantitatively shown to affect the zero-shear rate viscosity of monodisperse combs.[41] The combination of these parameters may lead to higher or lower viscosities compared to the linear reference with the same molar mass, depending on the opposite effects of side branches on the relaxation of the backbone: increased friction and tube dilation. The zero-shear rate viscosities of the synthesized combs are compared with linear PnBA chains in Figure 6.

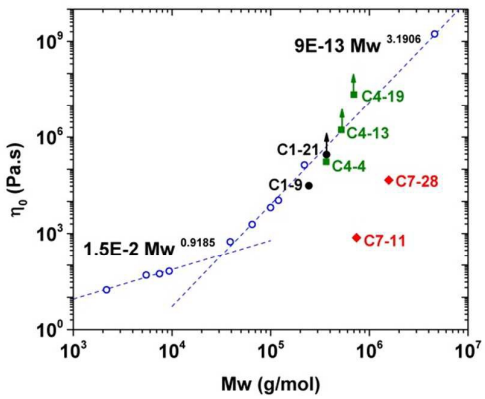

Figure 6. Comparing zero-shear rate viscosities of the synthesized combs and linear PnBA.

The zero-shear rate viscosities of linear chains are calculated from data given by Jullian et al.[31] The transition from unentangled to entangled regimes gives the Mc of about 30k which confirms the Me of 15k as suggested in this work. The zero-shear rate viscosities of moderately branched combs (C1 and C4 series with almost one and one third of an entanglement space between branches) with branches shorter than an entanglement almost reside on the behaviour expected from the linear equivalents. However, for branches longer than one entanglement, despite that the final Newtonian flow cannot be achieved in the measured frequency domain and the actual viscosity is above the maximum viscosity as determined in this plot, the zero-shear rate viscosity is above what could be attained with equivalent linear structures. On the other hand, for densely branched combs having one eighth of an entanglement distance between following branches, with both branch lengths below and above Me, the zero-shear rate viscosities are located far below their linear equivalents. In these cases the tube dilation effect dominates the final relaxation. Such an anomalously low zero shear-rate viscosities have been also reported for bottle-brushes as well.[12, 38, 39, 42] These observations are in agreement with Inkson's theoretical predictions.[41]

III.3 Remarks from theoretical prediction

Recently the time marching algorithm (TMA) developed by van Ruymbeke et al. based on traditional tube based models has been successfully applied to variety of complex polymer and supramolecular structures.[24, 43, 44] In order to have a better overview from the expected behaviour, we used TMA's three fluctuations modes (TFM) model developed for comb architectures[24] and study the effect of length and number of branches on such a system. The effective backbone in this model is defined as the longest end-to-end distance in the molecule, therefore if the length of the branches is longer than the segments between them, the effective backbone would have long branches at both extremities and the actual backbone extremities form short branches. Backbone segments can therefore fluctuate with respect to the first branch (short one) or the second branch (long one) carrying the short branch, or with respect to the middle of the backbone, carrying all branches placed in between. Short and long branches fluctuate just like arms of a star and final backbone reptation might be accelerated by tube dilation or postponed by the extra friction coming from the relaxed branches.[24] The consequence of this collation on the final relaxation of backbone through reptation or fluctuations is not trivial.

As a representative, Figure 7 compares the rheological properties of the comb structures equivalent to C7-11. The material parameters were adopted from linear backbones (Figure 2), i.e. $\boldsymbol{G_N^0}$ of 1.5×10^5 Pa, Me of 15 kg/mol and τ_e equal to 1×10^{-4} s. According to the number of initiating sites on the backbone and the conversion of the second step ATRP (Table 2), the expected structure has 68 branches with 11 kg/mol length. Since the length of side branches is lower than Me, they should relax by simple Rouse mechanism and won't make a discernible step in the relaxation spectrum (lines with triangles). This relaxation can be distinguished by the corresponding peak in the inset vGP plot. The moduli drop in parallel down to a level determined by diluted backbone. This behaviour is frequently reported for bottle-brush structures forming super-soft materials.[37-39, 42] If due to steric hindrance, only one third of the initiation sites find the chance to grow, almost 23 branches with 33 kg/mol length will be formed. As the length of branches is above 2Me, they form entanglements and a separate plateau modulus at high frequencies (lines with circles). Since the weight fraction of branches is not changed, the moduli drop down to the same level, but final relaxation is delayed due to higher friction from longer branches. In such a case, two separate plateaus can be distinguished, as could be also comprehended from two local minima in the inset vGP plot. Finally, if only one ninth of the initiation sites grow, 8 branches with

View Article Online
DOI: 10.1039/C6SM02576E

99 kg/mol length will be formed. The fluctuation time of the branches is even beyond reptation of the backbone precursor, as shown in Figure 7 (lines with squares). Since the relaxation times of the backbone and branches are not well separated (compare the branch relaxation peak and the small minimum corresponding to backbone entanglement in the corresponding vGP plot), the plateau corresponding to the entangled backbones is barely discernible. In conclusion, increasing the number of short branches accelerates final relaxation by further dilution, but longer branches at lower numbers may postpone relaxation by extra friction.

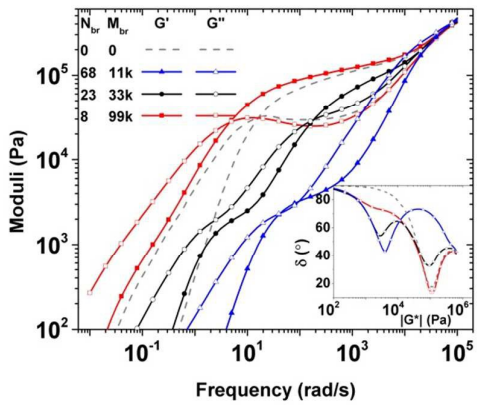

Figure 7. Theoretical predictions of dynamics moduli (main plot) and vGP (inset plot) of combs equivalent to the structure of C7-11.

The LVE and vGP plots of the C7-11 sample resemble the behaviour shown by the intermediate structure. Branches form a discernible plateau at high frequencies and a delicate backbone relaxation might be discernible at lower modulus levels after parallel drop of moduli. In other words, unlike the initial expectations, only few numbers of initiation sites (less than one third in case of C7-11) have had the chance to grow, and actual branches are longer than expectations. This fraction has been even lower for C1 and C4 series since their branches are well entangled and the backbone relaxation is less discernible, like the behaviour of the third structure in Figure 7. Coupling of several combs at higher branch lengths has led to gel like behaviour for longer branches. These results also confirm the observed behaviour of zero-shear rate viscosities.

In order to suggest a rough estimate from the length and number of side branches, a simple rheological model was developed based on TMA. In this model, the comb structure was replaced by a binary blend of monodisperse star and linear chains representing branches and backbone. Similar to the hierarchical relaxation mechanism of combs, branches were allowed to fluctuate from the beginning while the backbone had a very long relaxation time. All the other relaxation phenomena including high frequency Rouse relaxation, dynamic dilution and constraint release were also activated. Details of mechanisms involved in relaxation of blends of linear and star polymers and the algorithm for considering all at the same time are described elsewhere.[45] More information can be also found in the Supporting Information. Such a model can simply represent the dynamic moduli in the intermediate frequencies where branches mainly dominate the relaxation behaviour, without complications of backbone coupling and their hierarchical relaxation. The length and fraction of branch component can be adjusted by comparing theoretical curves to the experimental dynamic moduli of different comb series. The developed model was first verified by application on a series of well-defined and well-established polystyrene comb series to evaluate their branch length.[46] The obtained results, as given in the Supporting Information are in very good agreement with the experimental data. Modelling results for the comb samples synthesized in this work are compared to the measured moduli in Figure 8. Theoretical curves can capture the experimental measurements especially for C1 and C4 series. The fitted branch lengths are depicted in Table 3. Since backbone relaxations are either merged in the polydisperse branches relaxation (in case of few number of short branches) or reside out of the accessible frequency range (in case of large number of long branches), the corresponding fraction and lifetimes can be very flexible and not definitive and therefore these results are not included.

Table 3. Branch lengths required to capture rheological data and their corresponding number.

Sample	Fitted Mw_{branch} (kg/mol)	Expected N_{br}	Calculated N_{br}	Fraction (mol%) of active initiation sites
C1-9	60	10	2.8	28
C1-21	76	10	3.5	35
C4-4	83	34	1.6	5
C4-13	97	34	4.5	13
C7-11	39	68	19.3	28
C7-28	45	68	42.6	63

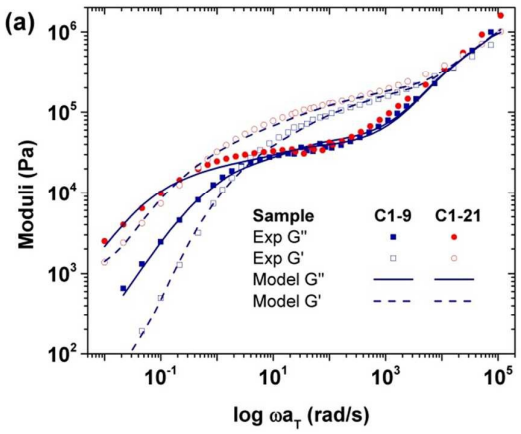

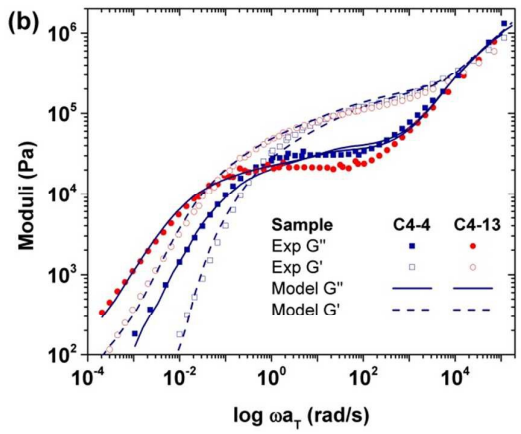

View Article Online
DOI: 10.1039/C6SM02576E

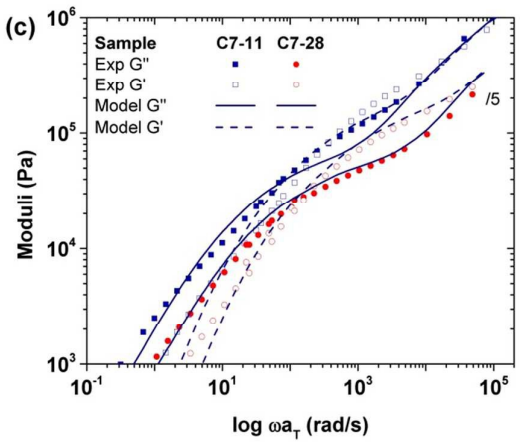

Figure 8. Comparing theoretical fits with experimental data for (a) C1 (b) C4 and (c) C7 comb series.

The average branch lengths required to capture the dynamic moduli in the intermediate frequencies are significantly longer than the ones calculated by considering participation of all potential initiation sites. Since the total fraction of branches is already known from the conversions obtained in the second ATRP step (Table 2) the corresponding number of branches can be calculated as shown in Table 3. The average fraction of active initiation sites are also shown in the last column. The obtained results nicely confirm the deductions made from Figure 7. C4 series samples has the longest branches and lowest number of branches, while in Sample C7-28 about two third of the initiation sites have been activated as depicted in the corresponding zero-shear rate viscosity. About one third of the intended branches are formed in the rest of the samples.

CRP methods are widely used in literature for synthesis of a variety of structures and they may yield products with well-defined structures. However, they have several limitations for the synthesis of complex architectures that may lead to higher structural dispersities. This is why the synthesis of complex architectures using CRP methods often involves separation of side products. However, there still might be considerable structural variation in the purified fraction as different structures may have similar hydrodynamic volume. This problem is much less present for the more controlled high vacuum anionic technique, but nevertheless still exists as recently proved by TGIC studies.[18, 19] This contribution demonstrates that comparison of theoretical predictions with the measured linear rheological behaviour provides a better insight in the synthesized structures that could not be easily obtained using the traditional characterization methods.

IV. Conclusions

Poly(n-butyl acrylate) combs with well-entangled backbone and moderate to densely branched structures are synthesized using ATRP in three steps including synthesis of backbone, cleavage of protecting groups and growth of side branches following a grafting-from approach. As expected, due to large number of branches and long backbones, coupling of combs and structural imperfections happen that cannot be easily distinguished by SEC. We have therefore tried to investigate rheological properties to provide better information from the actual microstructures. Rheological properties of linear samples shows a 0.15 MPa plateau modulus which corresponds to 15k entanglement length. Dynamic moduli curves show that for moderately branched samples with short branches, the final relaxation is postponed to lower frequency, while it has been accelerated compared to the linear backbone for densely branched comb. Zero-shear-rate viscosities of this series fall far below the corresponding value of the equivalent linear chains. Theoretical predictions of linear viscoelastic properties made by time marching algorithm show that dilution of backbone, after relaxation of short side branches, may accelerate final relaxation, while extra friction can postpone it especially for smaller number of long branches. The actual length and number of branches could be estimated by comparing predictions to the measured moduli in the intermediate frequency region where branch relaxation dominates the behaviour. This comparison reveals that only a small fraction of initiation sites has found the chance to grow, and a lower number of branches with lengths larger than expectations made from traditional characterization methods are formed.

Notes and references

1. F. J. Stadler, B. a. Arikan-Conley, J. Kaschta, W. Kaminsky and H. Münstedt, *Macromolecules*, 2011, **44**, 5053-5063.
2. D. Auhl, F. J. Stadler and H. Münstedt, *Rheologica acta*, 2012, **51**, 979-989.
3. R. Verduzco, X. Li, S. L. Pesek and G. E. Stein, *Chem. Soc. Rev.*, 2015, **44**, 2405-2420.
4. W. A. Braunecker and K. Matyjaszewski, *Progress in Polymer Science*, 2007, **32**, 93-146.
5. G. Cheng, A. Böker, M. Zhang, G. Krausch and A. H. Müller, *Macromolecules*, 2001, **34**, 6883-6888.
6. Y. Zhang, Z. Shen, D. Yang, C. Feng, J. Hu, G. Lu and X. Huang, *Macromolecules*, 2009, **43**, 117-125.
7. A. Nese, J. Mosnacek, A. Juhari, J. A. Yoon, K. Koynov, T. Kowalewski and K. Matyjaszewski, *Macromolecules*, 2010, **43**, 1227-1235.
8. J. Bolton and J. Rzayev, *ACS Macro Letters*, 2011, **1**, 15-18.
9. S. S. Sheiko, B. S. Sumerlin and K. Matyjaszewski, *Progress in Polymer Science*, 2008, **33**, 759-785.
10. Y. Tsukahara, S.-i. Namba, J. Iwasa, Y. Nakano, K. Kaeriyama and M. Takahashi, *Macromolecules*, 2001, **34**, 2624-2629.
11. S. Ohno and K. Matyjaszewski, *Journal of Polymer Science Part A: Polymer Chemistry*, 2006, **44**, 5454-5467.
12. H. Y. Cho, P. Krys, K. Szcześniak, H. Schroeder, S. Park, S. Jurga, M. Buback and K. Matyjaszewski, *Macromolecules*, 2015, **48**, 6385-6395.
13. S. J. Lord, S. S. Sheiko, I. LaRue, H.-I. Lee and K. Matyjaszewski, *Macromolecules*, 2004, **37**, 4235-4240.
14. P. Chambon, C. M. Fernyhough, K. Im, T. Chang, C. Das, J. Embery, T. C. McLeish and D. J. Read, *Macromolecules*, 2008, **41**, 5869-5875.
15. Y. Lin, J. Zheng, K. Yao, H. Tan, G. Zhang, J. Gong, T. Tang and D. Xu, *Polymer*, 2015, **59**, 252-259.
16. G. C. Berry, S. Kahle, S. Ohno, K. Matyjaszewski and T. Pakula, *Polymer*, 2008, **49**, 3533-3540.
17. M. Gerle, K. Fischer, S. Roos, A. H. Müller, M. Schmidt, S. S. Sheiko, S. Prokhorova and M. Möller, *Macromolecules*, 1999, **32**, 2629-2637.
18. F. Snijkers, E. Van Ruymbeke, P. Kim, H. Lee, A. Nikopoulou, T. Chang, N. Hadjichristidis, J. Pathak and D. Vlassopoulos, *Macromolecules*, 2011, **44**, 8631-8643.
19. E. Van Ruymbeke, H. Lee, T. Chang, A. Nikopoulou, N. Hadjichristidis, F. Snijkers and D. Vlassopoulos, *Soft matter*, 2014, **10**, 4762-4777.
20. M. Kapnistos, D. Vlassopoulos, J. Roovers and L. Leal, *Macromolecules*, 2005, **38**, 7852-7862.

View Article Online
DOI: 10.1039/C6SM02576E

21. K. M. Kirkwood, L. G. Leal, D. Vlassopoulos, P. Driva and N. Hadjichristidis, *Macromolecules*, 2009, **42**, 9592-9608.
22. J. H. Lee, P. Driva, N. Hadjichristidis, P. J. Wright, S. P. Rucker and D. J. Lohse, *Macromolecules*, 2009, **42**, 1392-1399.
23. J. H. Lee, L. J. Fetters and L. A. Archer, *Macromolecules*, 2005, **38**, 10763-10771.
24. M. Ahmadi, C. Bailly, R. Keunings, M. Nekoomanesh, H. Arabi and E. Van Ruymbeke, *Macromolecules*, 2011, **44**, 647-659.
25. M. Kapnistos, K. Kirkwood, J. Ramirez, D. Vlassopoulos and L. Leal, *Journal of Rheology (1978-present)*, 2009, **53**, 1133-1153.
26. M. Kempf, D. Ahirwal, M. Cziep and M. Wilhelm, *Macromolecules*, 2013, **46**, 4978-4994.
27. H. Lentzakis, D. Vlassopoulos, D. Read, H. Lee, T. Chang, P. Driva and N. Hadjichristidis, *Journal of Rheology (1978-present)*, 2013, **57**, 605-625.
28. N. M. Ahmad, B. Charleux, C. Farcet, C. J. Ferguson, S. G. Gaynor, B. S. Hawkett, F. Heatley, B. Klumperman, D. Konkolewicz and P. A. Lovell, *Macromolecular rapid communications*, 2009, **30**, 2002-2021.
29. C. Former, J. Castro, C. M. Fellows, R. I. Tanner and R. G. Gilbert, *Journal of Polymer Science Part A: Polymer Chemistry*, 2002, **40**, 3335-3349.
30. W. Radke and A. H. Müller, *Macromolecules*, 2005, **38**, 3949-3960.
31. N. Jullian, F. Leonardi, B. Grassl, J. Peyrelasse and C. Derail, *Appl. Rheol*, 2010, **20**, 33685.
32. L. Fetters, D. Lohse and R. Colby, in *Physical properties of polymers handbook*, Springer, 2007, pp. 447-454.
33. N. M. Ahmad, P. A. Lovell and S. M. Underwood, *Polymer international*, 2001, **50**, 625-634.
34. C. Liu, J. He, E. Van Ruymbeke, R. Keunings and C. Bailly, *Polymer*, 2006, **47**, 4461-4479.
35. S. M. M. Mortazavi, H. Jafarian, M. Ahmadi and S. Ahmadjo, *Journal of Thermal Analysis and Calorimetry*, 2016, **123**, 1469-1478.
36. F. J. Stadler, J. Kaschta and H. Münstedt, *Macromolecules*, 2008, **41**, 1328-1333.
37. M. Hu, Y. Xia, G. B. McKenna, J. A. Kornfield and R. H. Grubbs, *Macromolecules*, 2011, **44**, 6935-6943.
38. C. R. López-Barrón, P. Brant, A. P. Eberle and D. J. Crowther, *Journal of Rheology (1978-present)*, 2015, **59**, 865-883.
39. S. J. Dalsin, M. A. Hillmyer and F. S. Bates, *Macromolecules*, 2015, **48**, 4680-4691.
40. T. Pakula, Y. Zhang, K. Matyjaszewski, H.-i. Lee, H. Boerner, S. Qin and G. C. Berry, *Polymer*, 2006, **47**, 7198-7206.
41. N. Inkson, R. Graham, T. McLeish, D. Groves and C. Fernyhough, *Macromolecules*, 2006, **39**, 4217-4227.
42. W. F. Daniel, J. Burdyńska, M. Vatankhah-Varnoosfaderani, K. Matyjaszewski, J. Paturej, M. Rubinstein, A. V. Dobrynin and S. S. Sheiko, *Nature materials*, 2016, **15**, 183-189.
43. M. Ahmadi, L. G. Hawke, H. Goldansaz and E. Van Ruymbeke, *Macromolecules*, 2015, **48**, 7300-7310.
44. L. Hawke, M. Ahmadi, H. Goldansaz and E. Van Ruymbeke, *Journal of Rheology (1978-present)*, 2016, **60**, 297-310.
45. E. van Ruymbeke, S. Coppola, L. Balacca, S. Righi and D. Vlassopoulos, *Journal of Rheology (1978-present)*, 2010, **54**, 507-538.
46. J. Roovers and W. Graessley, *Macromolecules*, 1981, **14**, 766-773.

View Article Online
DOI: 10.1039/C6SM02576E

Graphical Abstract

Closer insight in the structure of moderate to densely branched combs by combining modeling and linear rheological measurements

Mostafa Ahmadi, Sandie Pioge, Charles-Andre Fustin, Jean-Francois Gohy, Evelyne van Ruymbeke